Glaciation of mixed-phase clouds by dry ice to cool the Arctic

Geordie Zapalac (Geordie.Zapalac@gmx.com)

Article

Keywords:

Posted Date: June 9th, 2023

DOI: https://doi.org/10.21203/rs.3.rs-2990551/v1

Additional Declarations: No competing interests reported.

Glaciation of mixed-phase clouds by dry ice to cool the Arctic

Geordie Zapalac
1000 Civic Center Dr Apt 4, Santa Cara, CA, 95050

Abstract

Arctic stratus or stratocumulus mixed-phase clouds have a substantial effect on the Arctic radiation budget[1] and winter sea ice growth is sensitive to long wavelength radiative forcing.[2] Clouds with a liquid water profile greater than 30 g m^{-2} are blackbody absorbers for terrestrial long wavelength radiation and increase the terrestrial forcing by roughly 40 W m^{-2} over clear skies or ice-only clouds.[1, 3] This report proposes glaciating Arctic mixed-phase clouds by seeding with dry ice during the winter months of November through February to restore summer sea ice and Arctic albedo. Seeding is performed by aircraft above the clouds dropping 1 kg km^{-1} of dry ice pellets in parallel tracks spaced by 1.2 km. Each track creates a curtain of ice crystals that diffuse through the cloud, glaciating the cloud by the Wegener-Bergeron-Findeisen process. The ice crystal and water vapor concentrations are simulated during a 4 day period after seeding for different assumptions of the eddy diffusion coefficient.

Introduction

The loss of sea ice accelerates Arctic warming and destabilizes the jet stream, causing heat waves, droughts, and floods at lower latitudes.[4] Arctic warming also melts the surface of the Greenland ice sheet causing sea level rise and weakening the oceanic thermohaline current.[5] Artificially cooling the Arctic to restore sea ice may be an effective strategy to reduce extreme weather events in the northern hemisphere during an interim period required to decarbonize the electricity grid and remove legacy CO_2 from the atmosphere.

Arctic sea ice is sensitive to long wavelength (LW) radiative forcing,[2] and low-level mixed-phase clouds have a pronounced effect on the Arctic radiation budget. Mixed-phase clouds containing super-cooled liquid water increase the LW forcing by roughly 40 W m^{-2} over clear skies or ice-only clouds,[1, 3] warming the Arctic surface by about 13 K.[6] On average, Arctic mixed-phase clouds increase the LW forcing at the Arctic surface by 30 W m^{-2} during the fall, winter, and spring.[7] Cloud glaciation during these months could cool the Arctic surface beneath the clouds by allowing roughly 40 W m^{-2} of LW terrestrial radiation to escape into colder, higher regions of the atmosphere or into space (Fig. 1).

This report proposes glaciating low-level mixed-phase clouds during November through February by seeding from above the cloud deck with pellets of dry ice, increasing the sea ice thickness during the Arctic winter and thereby increasing the reflective area of sea ice during the summer. The report also details an elementary simulation in the Methods section, developed specifically to model the glaciation of an Arctic mixed-phase cloud by dry ice, in order to estimate the amount of dry ice required per km^{-2} to glaciate the clouds. The simulation is not an LES model; it assumes an effective eddy diffusion coefficient for the ice crystals and integrates the diffusion equation in short time steps, allowing the ice crystals to settle by including an advection term.

There are other proposals to cool the Arctic. Stratospheric aerosol injection of SO_2 north of 60° N latitude during spring would reduce short wave (SW) solar radiative warming of the Arctic during the summer.[8] A proposal called Arctic Ice Management would pump seawater onto sea ice during the winter so that it freezes, thickening the ice to prevent it from melting away entirely during the summer.[9] Applying a thin layer of hollow glass microspheres over newly formed sea ice would increase the ice albedo from 30% to 80% so that new ice is less likely to melt during the summer.[10] Marine Cloud Brightening[11] has been proposed to brighten Arctic clouds during the summer to enhance the cooling by increasing the reflection of SW radiation.[12] The cooling method discussed here is complementary to each of these other proposals.

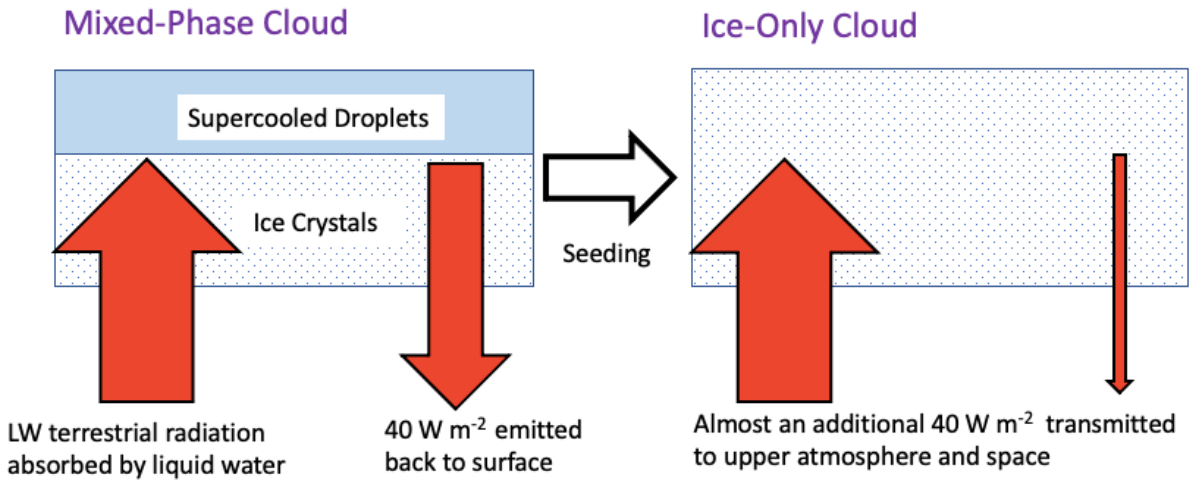

Figure 1. Glaciation of an Arctic mixed-phase cloud by seeding. The ice-only cloud allows more LW terrestrial radiation to escape from the Arctic surface into the higher atmosphere or into space, cooling the surface.

Radiative forcing and sea ice growth

The warming effect of clouds on the Arctic surface is demonstrated most easily during winter when SW solar radiation may be neglected; for LW radiation the cloud reflectance is negligible, considerably simplifying the cloud's optical properties. The optical path of LW radiation through a cloud depends upon the liquid water path LWP within the cloud and is given approximately by $\tau_C = k_e \mathrm{LWP}$, where LWP is in units of g m^{-2} and $k_e = 0.156$ m^2 g^{-1} is the mass extinction coefficient.[13] For mixed-phase clouds we neglect the contribution of ice crystals to the optical path under the assumption that the ice crystals have a much lower number concentration than the liquid water droplets. The cloud LW transmittance is $t_C = e^{-\tau_C}$ so that the LW absorption, or equivalently the cloud emissivity, is given by $\varepsilon_C = 1 - \exp(-k_e \mathrm{LWP})$. For liquid water profiles greater than 30 g m^{-2}, a common condition for low-level Arctic mixed-phase clouds, $\varepsilon_C > 0.99$ and the cloud is effectively a blackbody absorber.

Snow and ice have an emissivity close to 1 for LW radiation so that the surface cooling is given by $F^{\uparrow} = \sigma T_S^{\,4}$, where σ is the Stefan-Boltzmann constant and T_S is the surface temperature. The LW downwelling or forcing from a clear Arctic sky may be approximated by $F^{\downarrow} = \varepsilon_E \sigma T_A^{\,4}$, where

T_A is an effective clear sky temperature and ε_E is an effective clear sky emissivity.[14] The net surface forcing is $F^{\text{net}} = F^{\downarrow} - F^{\uparrow} = \sigma\left(\varepsilon_E T_A^4 - T_S^4\right)$. During an Arctic winter under clear skies we may set, for example, $T_S = 240$ K, $T_A = 235$ K, and $\varepsilon_E = 0.7$, yielding $F^{\text{net}} =$ -67 W m^{-2}.[14] If a mixed-phase cloud is present we replace the effective clear sky emissivity ε_E with the cloud emissivity $\varepsilon_C = 1$ so that $F^{\text{net}} = \sigma\left(T_C^4 - T_S^4\right)$, where T_C is the cloud temperature, which is usually close to the surface temperature. $T_C = 238$ K yields $F^{\text{net}} =$ -6.2 K so that the surface warming from downwelling LW radiation in this example is 61 W m^{-2} less under clear skies than under cloudy skies.

A reduction in LW radiative forcing $\Delta F^{\uparrow}$ applied over a time period t would increase the sea ice thickness Δh by approximately $\Delta h = F^{\uparrow} t / (\rho L)$, where $L = 333.4$ kJ kg^{-1} is the latent heat of fusion of seawater and $\rho = 917$ kg m^{-3} is the density of sea ice.[15] This simple estimate predicts that 1 W m^{-2} of reduced forcing sustained for 1 month will thicken the sea ice by 0.85 cm. Lui and Key present evidence that the September Arctic sea ice coverage increased 48% between 2012 and 2013 due to a 20% reduction in cloud coverage during January and February in 2013.[15]

Seeding Arctic mixed-phase clouds

On average, mixed-phase stratus or stratocumulus clouds cover 36% of the Arctic surface area during the 4-month period from November through February.[16] Arctic mixed-phase clouds have a layer of super-cooled liquid droplets in the top part of the cloud and a layer of more diffuse and larger ice crystals beneath the droplet layer (Fig. 2).[3] The cloud base is usually within 2 km of the Arctic surface and the cloud liquid layer thickness varies with season, from sometimes nearly absent during the winter to 400-700 m thick during the fall.[17] The cloud top is usually located below a humidity inversion, and water vapor advected above the cloud plays an important role in sustaining the cloud if it is located over pack ice rather than open ocean.[18] Arctic mixed-phase clouds are remarkably stable against spontaneous glaciation by the Wegener-Bergeron-Findeisen (WBF) process for up to 2 weeks.[3]

The stability of Arctic mixed-phase clouds is believed to originate from cloud-top radiative cooling caused by LW emission from the liquid droplet layer.[3] The radiative cooling creates turbulence within the cloud that causes updrafts and downdrafts. During an updraft a rising air parcel expands adiabatically and cools, so that the vapor pressure is greater than both the ice and liquid saturation vapor pressures. Water vapor condenses on the abundant cloud condensation nuclei (CCN), replenishing droplets that have evaporated due to the WBF process. The CCN concentration (~100 cm^{-3}) is roughly a factor 10^6 higher than the natural concentration of ice nucleation particles (INP) of ~0.1 L^{-1}.[3] Because the liquid and ice layers are separated in Arctic clouds and INP are scarce, ice crystals growing within the liquid cloud layer by the WBF process tend to precipitate out before the liquid droplet layer is glaciated. The INP concentration required to tip the cloud into a completely glaciated state has been simulated to be 10 L^{-1} or about 100 times the natural INP concentration.[19]

Cloud glaciation by seeding usually dispenses silver iodide particles to increase precipitation. However, iodine can react with ozone in the atmosphere to create iodic acid, a potent component of CCN that might act to increase the liquid droplet concentration in clouds and thereby increase the warming of the Arctic surface.[20] For this reason and because of cost, this proposal considers seeding by dropping 3 mm diameter cylindrical dry ice pellets above the cloud. As the pellet sublimates it freezes the surrounding water vapor and leaves behind a trail of ice crystals that serve as embryos for vapor deposition by the WBF process.[21] One kilogram of dry ice pellets can generate about 10^{15} ice crystals that grow to critical mass before the pellet sublimates completely.[21, 22]

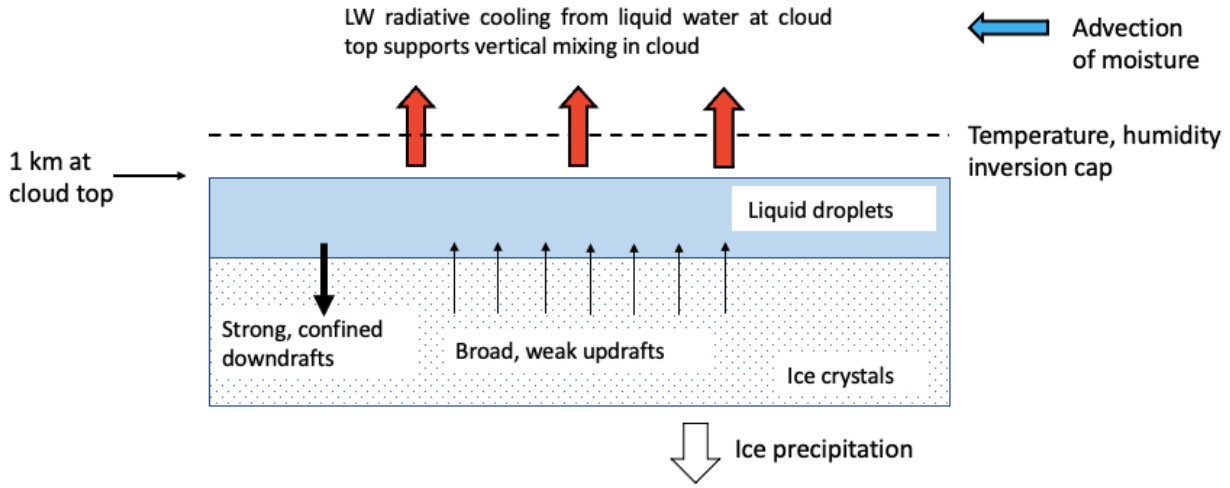

Figure 2. Organization of an Arctic mixed-phase cloud.

The liquid water content of mixed-phase clouds is lowest during the coldest months of the year, however all clouds with LWP > 30 g m^{-2} are blackbody emitters and have an equivalent effect on the LW radiation budget. Therefore, the most cost-effective seeding is during the Arctic winter months of November through February when the least amount of seeding agent can be applied to fully glaciate the clouds. Ice crystal number production from a falling dry ice pellet is also more efficient during the colder winter temperatures.[22]

Once glaciated by seeding, cloud-top radiative cooling nearly ceases so that the in-cloud turbulence is greatly reduced. Under the condition of reduced turbulence, most of the ice crystals gradually precipitate over a period of several hours. After the ice crystals are gone, a mixed-phase cloud is expected to eventually reform after sufficient water vapor diffuses into the original glaciated region. However, the entrainment of moisture into the glaciated region occurs very slowly under the condition of reduced turbulence.

Dry ice required to seed the Arctic

The cost for cooling the entire Arctic north of 70° N, an area of 15.4×10^6 km^2, ultimately depends upon the dry ice kg km^{-2} required to glaciate the clouds. To estimate this quantity an elementary simulation was written to provide the results for this section. The budget and logistics for manufacturing and deploying a dedicated fleet of aircraft to perform the seeding is beyond the

scope of this report. The cost to cool the Arctic for the entire winter depends on the average frequency that the same region must be re-seeded because mixed-phase clouds will probably reform after a few days. This frequency is assumed to be every 4 days in this section, but it would have to be determined by field experiments.

In the thought experiment for this section, cloud seeding is done using a fleet of airships over a winter mixed-phase cloud with a 200 m thick liquid droplet layer, corresponding to a LWP of 83.6 g m^{-2}. The airships drop 1 kg km^{-1} of dry ice pellets immediately above the top of the clouds in tracks separated by a distance $S = 1.2$ km. The ice pellets are cylindrical with an initial diameter of 0.3 cm and an average length of 1.0 cm. For these pellet dimensions, 91% of the pellet has sublimated after falling through 400 m (see the Methods section). As a dry ice pellet descends it creates a dense trail of ice embryos by homogeneous vapor nucleation. 10^{15} ice embryos per kg of dry ice grow to critical mass before sublimating. Part of these ice crystals grow within the saturated environment of the cloud and evaporate the liquid droplets by the WBF process. After 12 hours most of the ice crystals have settled to the ground. New moisture is assumed to advect laterally at a distance of 200 m above the original cloud, but this moisture is slow to entrain vertically because the eddy diffusion coefficient is much smaller after glaciation. The diffusion of the water vapor and ice crystals, and the growth and subsidence of the ice crystals, are modelled with the simulation described in the Methods section.

The simulation uses an effective eddy diffusion coefficient D that is estimated from the measured turbulent energy dissipation rate ε by the relation $D = 0.8\varepsilon / \omega_B^{\,2}$, where ω_B is the Brunt-Väisälä frequency, estimated here to be 0.01 s^{-1}.[23] Shupe et al. have measured highly variable turbulent dissipation rates that are typically 10^{-5} to 10^{-3} m^2 s^{-3} for Arctic mixed-phase clouds during the fall,[17] with observed values as low as 10^{-6} m^2 s^{-3}. The simulation assumes a turbulent dissipation rate of 10^{-3} m^2 s^{-3} for the initial mixed phase cloud, or an eddy diffusion coefficient D_0 of 8 m^2 s^{-1}. The turbulent dissipation rate for a glaciated cloud is not known, but it is expected to be much smaller than 10^{-3} m^2 s^{-3} because cloud-top radiative cooling will be greatly reduced after the cloud is glaciated. The simulation explores two values near the low end of the measurements by Shupe et al.: 10^{-6} m^2 s^{-3} and 10^{-5} m^2 s^{-3}. These values correspond to glaciated cloud eddy diffusion coefficients D_G of 0.008 m^2 s^{-1} and 0.08 m^2 s^{-1}.

Fig. 3 shows the ice crystal concentration from the simulation at intervals of 2 minutes, 1 hour, 6 hours, and 12 hours after seeding, for $D_0 = 8$ m^2 s^{-1} and $D_G = 0.08$ m^2 s^{-1}. For this plot the source plane is at $x = 0$, the initial liquid droplet layer is between $-400 \le x \le -200$ m, and the ground is at $x = -1200$ m. The dry ice is deployed at $z = 0$ and $x = -200$ m and the air temperature is -20 °C . The units of concentration shown are 10^7 particles m^{-3}. The contours show that the core of the ice crystal distribution spreads and subsides to the ground over a period of about 12 hours. The clouds are seeded by tracks separated by $S = 1.2$ km. Fig. 4 shows the corresponding water vapor concentrations.

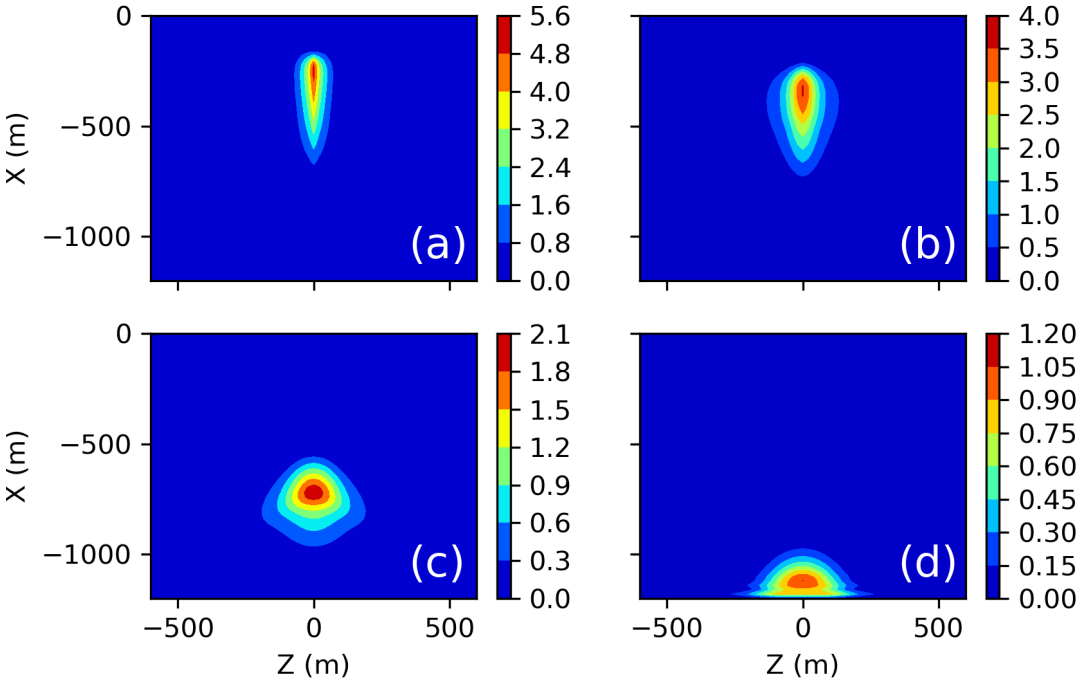

Figure 3. Concentration of ice crystals (10^7 particles m^{-3}) after seeding at x = -200 m. The ice pack is at x = -1200 m at the bottom of the plots. The cloud has an initial eddy diffusion coefficient of D_0 = 8 m^2 s^{-1} and a glaciated cloud eddy diffusion coefficient of D_G = 0.08 m^2 s^{-1}. The time intervals shown after seeding are (a) 2 minutes, (b) 1 hour, (c) 6 hours, and (d) 12 hours.

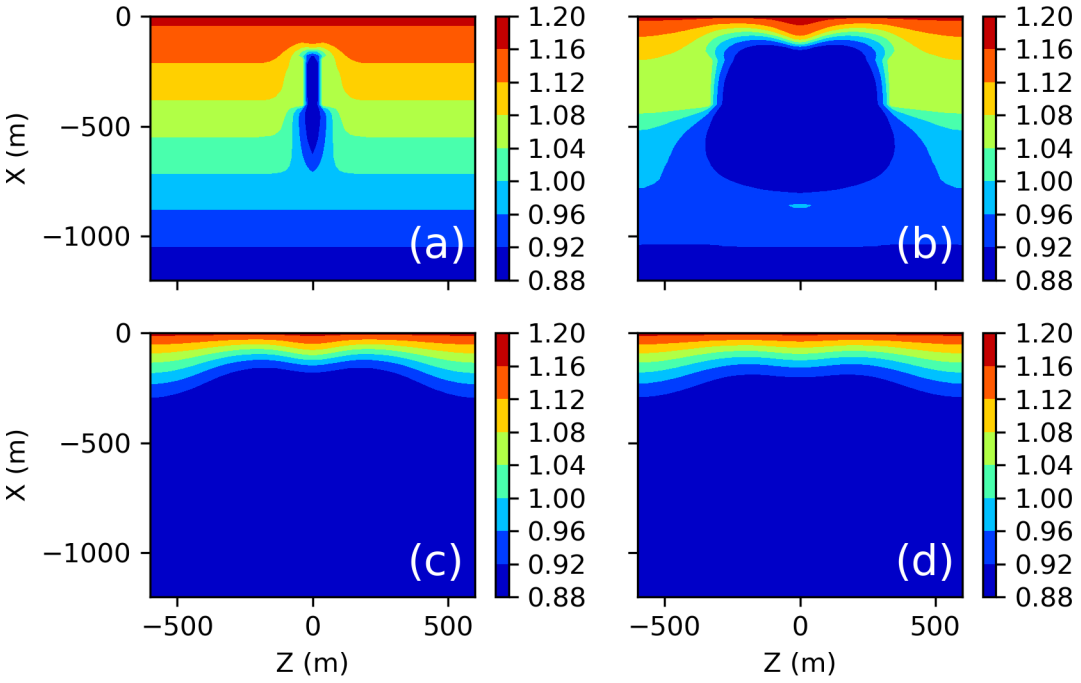

Figure 4. Water vapor concentration (g m^{-3}) for the same conditions as Fig. 3 at (a) 2 minutes, (b) 1 hour, (c) 6 hours, and (d) 12 hours after seeding.

Fig. 5 shows the LWP at the same four time intervals as in Figs. 3 and 4 to show the progress of cloud glaciation. These contour plots show minutes after seeding versus z position. If the cloud is seeded using tracks separated 2.4 km instead of 1.2 km, the glaciation only extends to about ± 600 m so that half of the clouds between the tracks remain unglaciated.

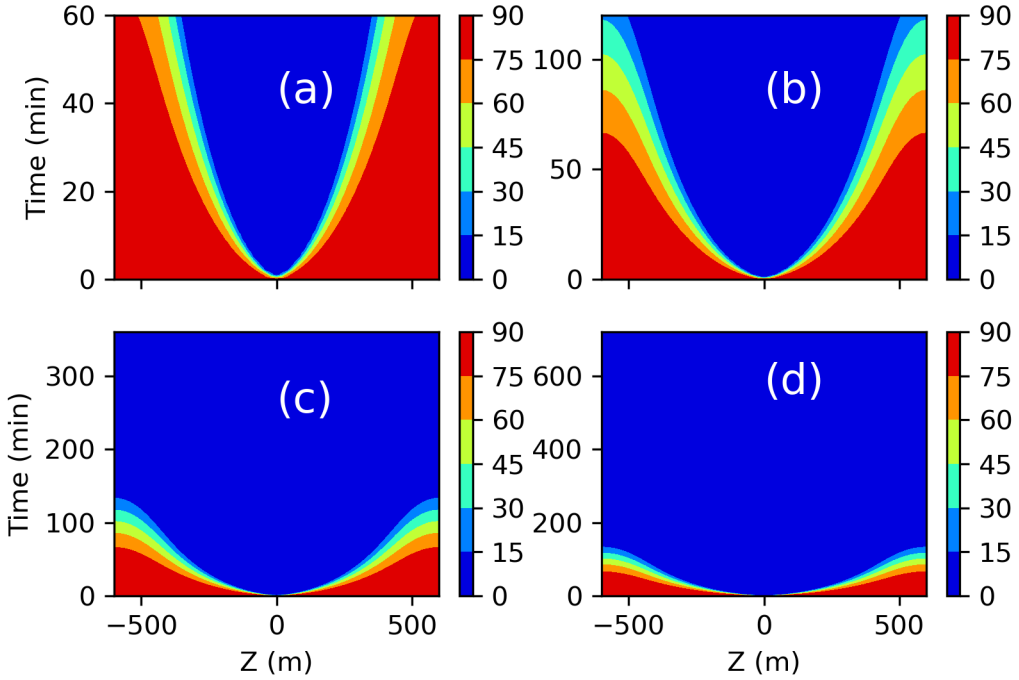

Figure 5. LWP (g m^{-2}) versus time at (a) 1 hour, (b) 2 hours, (c) 6 hours, and (d) 12 hours after seeding.

Figure 6 shows the water vapor concentration after 4 days for $D_G = 0.08$ m^2 s^{-1} and $D_G = 0.008$ m^2 s^{-1}. Although glaciation happens rapidly and most of the ice crystals settle to the ground after a few hours, water vapor from the source plane at $x = 0$ m entrains very slowly into the original cloud region below $x = -200$ m because of the small value of D_G. It is not known how long this condition persists on average before a synoptic disturbance, for example, accelerates the mixing so that the original cloud can reform.

A single airship traveling at 150 km h^{-1} could seed an area of 17280 km^2 in 4 days if the width of the glaciated region behind the airship were 1.2 km. Seeding the entire Arctic region north of 70° N would therefore require at least 890 airships if it were reseeded every 4 days.

Conclusions

The simulation indicates that Arctic mixed-phase clouds with an effective diffusion coefficient of 8 m s^{-2} may be glaciated with 0.83 kg km^{-2} of dry ice, where the dry ice pellets are dropped by an aircraft above the clouds at 1 kg km^{-1}, and that the glaciated region spreads to a width of 1.2 km. This region is mostly glaciated after 2 hours and most of the ice crystals created by the dry ice settle to the ground after 12 hours, but entrainment of sufficient advected moisture from above the

original clouds to reform new clouds should take much longer because the effective diffusion coefficient for the glaciated cloud is at least 100 times smaller. The average time before the clouds reform would have to be determined by future field experiments, and it is hoped that the results from this report, including the simulation code provided with the report, will help to de-risk such an experiment.

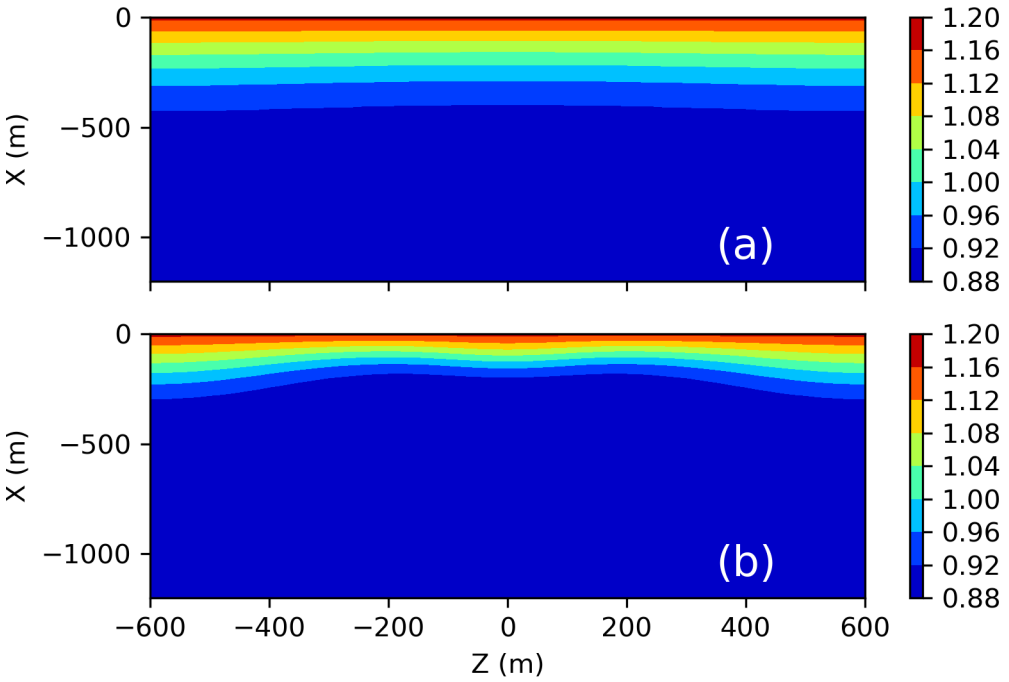

Figure 6. Water vapor concentration (g m^{-3}) 96 hours after seeding for two values of the eddy diffusion coefficient after glaciation: (a) D_G = 0.08 m^2 s^{-1}, and (b) D_G = 0.008 m^2 s^{-1}. The water vapor concentration is saturated at 1.075 g m^{-3}.

Arctic cloud glaciation is probably a more benign intervention than stratospheric aerosol injection or marine cloud brightening. If those interventions were suddenly interrupted much of the global heating avoided would return within days or weeks. By contrast, Arctic cloud seeding primarily cools the earth through the slow feedback of thickening the sea ice during the winter so that the Arctic albedo increases during the summer. If interrupted after a few years, it should require a comparable number of years for the sea ice to melt back to its original surface area. Furthermore, there is a negligible change to the SW radiation affecting the Arctic ecosystem because seeding is only performed during the darkest months of the year.

Future investigation into this topic should include an LES simulation of seeding, and a pan-Arctic climate simulation to evaluate the effects of dry ice cloud seeding on the sea ice surface area over several years. Dry ice seeding may also be effective for restoring sea ice near the south pole. Most important, as already emphasized above, are field experiments to evaluate the efficacy of the method, and to compare the simulations with experimental results.

References

1. M. D. Shupe, J. M. Intrieri (2004). Cloud radiative forcing of the Arctic surface: the influence of cloud properties, surface albedo, and solar zenith angle. *J. Clim*., 17, p. 616.
2. E. E. Ebert, J. A. Curry (1993). An intermediate one-dimensional thermodynamic sea ice model for investigating ice-atmosphere interactions. *J. Geophys. Res.*, 98, 10,085-10,109.
3. H. Morrison, et al. (2012). Resilience of persistent Arctic mixed-phase clouds. Nat. Geosci., 5, 11.
4. J. A. Francis, S. J. Vavrus (2012). Evidence linking Arctic amplification to extreme weather in mid-latitudes. *Geophys. Res. Lett.* 39, L06801.
5. P. Wadhams (2017). *A Farewell to Ice, A Report from the Arctic*. Oxford University Press.
6. K. Stramler, A. D. Del Genio, W. B. Rossow (2011). Synoptically driven Arctic winter states. *J. Clim*., 24, p. 1747.
7. J. Intrieri et al. (2002). An annual cycle of Arctic cloud forcing at SHEBA. *J. Geophys. Res*., 107, doi.org/10.1029/2000JC00423.
8. W. R. Lee, D. G. MacMartin, D. Visioni, B. Kravitz (2021). High-latitude stratospheric aerosol geoengineering can be more effective if injection is limited to spring. *Geophys. Res. Lett.*, 48, e2021GL092696.
9. S. J. Desch et al. (2016). Arctic ice management. *Earth's Future*, 5(1), p. 107.
10. L. Field et al. (2018). Increasing Arctic sea ice albedo using localized reversible geoengineering. *Earth's Future*, 6, p. 882.
11. J. Latham et al. (2008). Global temperature stabilization via controlled albedo enhancement of low-level maritime clouds. *Phil. Trans. R. Soc. A*., 372(1882), 3969-87.
12. B. Kravitz et al. (2014). Process-model simulations of cloud albedo enhancement by aerosols in the Arctic. *Phil. Trans. R. Soc. A.*, 372, 20140052.
13. G. L. Stephens (1978). Radiation profiles in extended water clouds. II: Parameterization schemes. *J. Atmos. Sci.*, 35, 2132.
14. G. W. Petty (2006). *A First Course in Atmospheric Radiation.* Sundog Publishing.
15. Y. Lui, J.R. Key (2014). Less winter cloud aids summer 2013 Arctic sea ice return from 2012 minimum. *Environ. Res. Lett*., 9, 044002.
16. J. Intrieri, et al. (2002). An annual cycle of Arctic cloud characteristics observed by radar and lidar at SHEBA. *J. Geophys. Res.*, 107, doi.org/10.1029/2000JC000423.
17. M. D. Shupe, P. Kollias, P. Ola G. Person, G. M. McFarquhar (2008). Vertical motions in Arctic mixed-phase stratiform clouds, *J. Atmos. Sci.*, 65, 1304-1322.
18. S. Qiu, Dong, B. Xi, J.-L. F. Li (2015). Characterizing Arctic mixed-phase cloud structure and its relationship with humidity and temperature inversion using ARM NSA observations. *J. Geophys. Res. Atmos.*, 120, 7737-7746.
19. K. Loewe, thesis, Karlsruher Institut für Technologie (2017).
20. A. Baccarini et al. (2020). Frequent new particle formation over the high Arctic pack ice by enhanced iodine emissions. *Nat. Commun.*, 11 (1), doi: 10.1038/s41467-020-18551-0.
21. A. S. Dennis (1980). *Weather Modification by Cloud Seeding.* International Geophysics Series, 24.
22. B. J. Morrison, thesis, Colorado State University (1989).
23. Y.-F. Wu, H.-U. Widdel (1989). Turbulent energy dissipation rates and eddy diffusion coefficients derived from foil cloud measurements, *J. Atmos. Terr. Phys.*, 51(6), 497-506.

Methods

Sublimation of a falling dry ice pellet

A cylindrical dry ice pellet with initial diameter $D_i = 0.3$cm and length $L = 1.0$cm is released at rest and accelerates to terminal velocity according to the following equation of motion:

$$m(t)\frac{du(t)}{dt} = m(t)g - \frac{1}{2}D(t)L\rho_a C_D u(t)^2 \tag{1}$$

where the time dependence of the pellet mass $m(t)$ and the pellet diameter $D(t)$ account for the sublimation of the pellet, L is the length of the pellet, $u(t)$ is the velocity of the pellet, $C_D = 0.82$ is the dimensionless drag coefficient for a long cylinder, ρ_a is the density of air, and g is the acceleration of gravity. In this treatment the diameter decreases as the pellet sublimates but the pellet length L remains constant.[24] Using this assumption the terminal velocity of the pellet is time-dependent and given by:

$$u_\infty(t) = \sqrt{\frac{\pi D(t)\rho_c g}{2\rho_a C_D}} \tag{2}$$

where $\rho_c = 1.4$ g cm^{-3} is the density of the pellet. To compute the pellet velocity after each time step dt we use the following explicit integration:

$$u(t+dt) = u(t) + \left[1 - \left(\frac{u(t)}{u_\infty(t)}\right)^2\right] g dt \tag{3}$$

During a time interval of dt seconds, Kochtubajda and Lozowski[24] calculate that a cylindrical ice pellet in an air stream at temperature T_a (°C) with velocity u cm s^{-1} will sublimate from an initial diameter of D_i cm to a final diameter D:

$$D = \left\{ D_i^{1.4} - \frac{0.73 k_a u^{0.6} dt}{\rho_c L_{sd} \nu_a^{0.6}} \left[T_a - T_s + \left(\frac{\mathrm{Pr}}{\mathrm{Sc}}\right)^{0.63} \frac{\varepsilon L_{sw}}{P C_p} e_a \right] \right\}^{1/1.4} \tag{4}$$

where $k_a = 2.43\times10^{-3} + 7.3\times10^{-6} T_a$ W cm^{-1} is the thermal conductivity of air, $T_s = -100$ °C is the surface temperature of the pellet, L_{sd} = 571 J g^{-1} is the specific latent heat of sublimation for dry ice, $\nu_a = \left(1.718\times10^{-4} + 5.1\times10^{-4} T_a\right)/\rho_a$ cm^2 s^{-1} is the kinematic viscosity of air, Pr = 0.69 is the Prandtl number for air, Sc = 0.61 is the Schmidt number for water vapor in air, ε = 0.622 is the ratio of molecular weights for water and air, $P = 97700$ Pa is the pressure at 1 km (the height

of the cloud base), $C_p = 1.005$ J g^{-1} °C^{-1} is the specific heat capacity of air, L_{sw} J g^{-1} is the specific latent heat of sublimation for ice, and e_a is the saturation vapor pressure of water in Pa. Kochtubajda and Lozowski provide L_{sw} and e_a as polynomial functions of T_a:

$$L_{sw}(T_a) = 2834 - 0.284826T_a - 5.05899\times10^{-3}T_a^2 - 2.16924\times10^{-5}T_a^3 + 1.04359\times10^{-7}T_a^4 \quad (5.a)$$

$$e_a(T_a) = 610.780 + 44.3652T_a + 1.42895T_a^2 + 0.0265065T_a^3 + 3.03124\times10^{-4}T_a^4 \quad (5.b)$$

Fig. 7(a) shows a simulation using Eqs. (1) – (5) for the diameter of the pellet as a function of the distance fallen at $T_a = -20$ °C. 8.9% of the pellet mass remains after the pellet has fallen 400 m. Fig. 7(b) shows the fraction of pellet mass that sublimates in each 20 m segment of the pellet trajectory; all of the points in Fig. 7(b) sum to 100%.

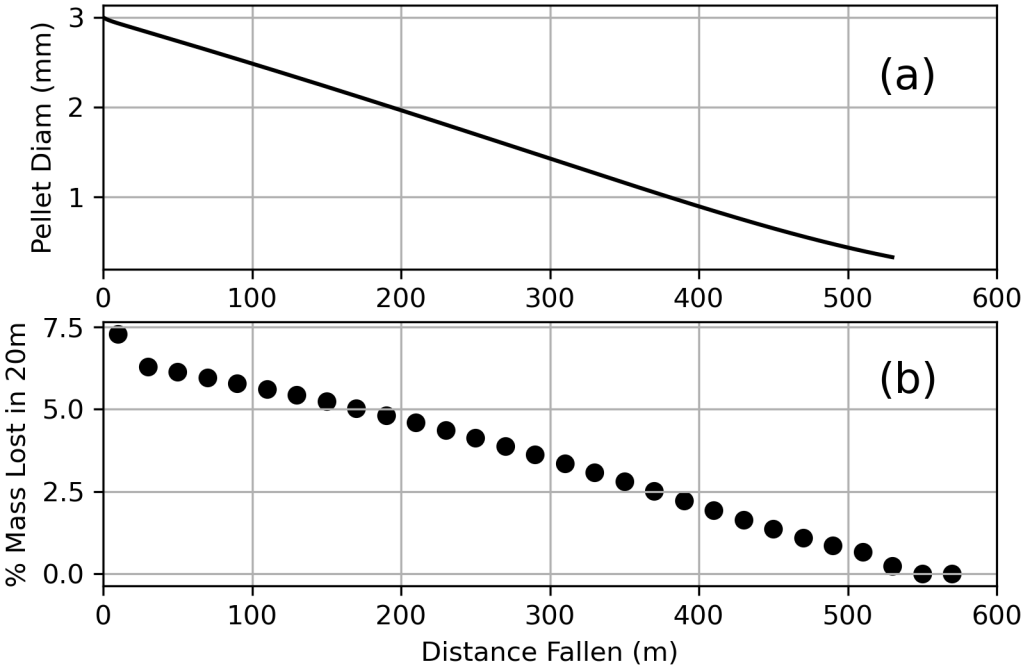

Figure 7. (a) Diameter of a falling cylindrical dry ice pellet as a function of fallen distance at -20 °C. (b) Percent of the pellet mass that sublimates in each 20 m segment of the falling pellet trajectory.

Simulation of the Arctic mixed-phase cloud after seeding

A heuristic simulation was written in C++ to estimate the time-dependent diffusion and subsidence of seeded ice crystals within a winter mixed-phase cloud using a two-dimensional grid normal to the flight direction of the seeding aircraft. The coordinate system extends vertically downwards from $x = 0$, the source plane for water vapor, to $x = 1200$ m at the ice pack (ground), and extends

laterally from $z = -600$ m to $z = +600$ m. The simulation explicitly solves for the ice crystal number concentration $C(x,z,t)$, the water vapor concentration $E(x,z,t)$, and the normalized distribution of ice crystal radii $\Gamma(x,z,t,r)$ at each grid location.

The grid uses a mesh size of $dx = dz = 20$ m with a time step of $dt = 1$ s. The binning of the ice crystal radii is more involved and discussed below. Water droplets occupy the region $200 < x < 400$ m, defining the liquid droplet cloud. At $t = 0$ dry ice is released at $x = 200$ m, $z = 0$ m at the top of the cloud. The temperature and pressure for the entire domain are approximated as constant values of $T = -20\,^{\circ}$C and $p = 90$ kPa. In the contour plots displayed in the main text this domain is shown as extending from $x = 0$ at the source plane to $x = -1200$ at the ice pack.

The initial condition for the water vapor concentration is calculated by solving the diffusion equation for the water vapor concentration using a diffusion coefficient of $D_0 = 8.0$ m^2 s^{-1}. At x = 0 (200 m above the top of the cloud) a Neumann boundary condition (B. C.) is implemented using Fick's Law $J_S = -D_0 \partial E / \partial x$ with a source term $J_S = 1.91 \times 10^{-6}$ kg m^{-2} s^{-1}. This source would eventually create 5.0 cm of snowfall per month, assuming that the snow is 1/10 the density of liquid water. At the ice pack ($x = 1200$ m) there is a Dirichlet B. C. requiring the water vapor pressure to equal the ice saturation vapor pressure e_i. The solution of the diffusion equation yields a linear dependence for the initial water vapor concentration. For these conditions the water vapor pressure equals the liquid saturation vapor pressure e_s at $x = 400$ m or a water vapor concentration of 1.075 g m^{-3} at $-20\,^{\circ}$C; this position is the lower bound of the liquid droplet cloud. At the source plane the water vapor concentration is 1.172 g m^{-3}. This concentration is applied as a Dirichlet B. C. for the water vapor for $t > 0$. It is assumed that water vapor at this concentration is advected laterally above the source plane and entrained into the domain of the simulation ($x > 0$ beneath the source plane) by turbulence as modeled by the eddy diffusion coefficient D.

In the liquid droplet region there are 10^8 droplets m^{-3} with a radius at $t = 0$ of 10 microns, corresponding to an initial liquid water profile $\mathrm{LWP}_0 = 83.6$ g m^{-2}. The droplets are not tracked in vertical position during the simulation. The droplets uniformly occupy the region $200 < x < 400$ m at all times before the cloud is glaciated, and all the droplets in a vertical column have the same size. As the simulation progresses the droplets uniformly evaporate; when the droplet radius reaches zero in a column the cloud is glaciated at the corresponding z position.

$\mathrm{LWP}(z)$, calculated from the droplet radius, determines the cloud emissivity[13] that drives the cloud-top radiative cooling. The radiative cooling in turn creates air turbulence that determines the eddy diffusion coefficient $D(z)$. This is modeled by allowing $D(z)$ to be proportional to the cloud emissivity, which is calculated from $\mathrm{LWP}(z)$:

$$D(z) = D_G + (D_0 - D_G)\frac{1 - \exp\left[-k_e \mathrm{LWP}(z)\right]}{1 - \exp\left[-k_e \mathrm{LWP}_0\right]} \qquad (6)$$

The initial value of the diffusion coefficient $D_0 = 8$ m^2 s^{-1} corresponds to the initial liquid water profile LWP_0 in Eq. (6). After the droplet radius reaches 0, $\mathrm{LWP}(z) = 0$ and $D(z) = D_G$. D_G is

the diffusion coefficient for an ice-only cloud. D_G is not known, so the simulation was run with assumptions of 0.08 m^2 s^{-1} and 0.008 m^2 s^{-1}, as discussed in the main text.

At $t = 0$ each kg of dry ice generates 10^{15} ice crystals that are distributed vertically according to Fig. 7(b). The initial ice crystal radius distribution is a log-normal distribution:

$$\Gamma(s) = \frac{1}{N} e^{-\frac{(s-\mu)^2}{\sigma^2}} \tag{7}$$

where $s = \log_{10}(r)$ with the ice crystal radius r in nanometers, $\mu = 1$ (corresponding to 10 nm), $\sigma = 0.2$, and N is a normalization constant: $\sum_{k=0}^{n_r-1} \Gamma(s_k) = 1$. There are $n_r = 500$ bins for s that range from 0 (1 nm) to 5 (100 microns). This is a smooth initial distribution roughly consistent with a critical radius of 9 nm at $-20\,°\text{C}$.[25] Exposed to water vapor, the spherical ice crystals increase in mass at the rate[26, 27]:

$$\frac{dm}{dt} = \frac{2\pi r(e/e_i - 1)}{\left[\frac{L_S^{\,2}}{R_v k_a T} + \frac{R_v T}{e_i \mathrm{D}_v}\right]} \tag{8}$$

where e/e_i is the ratio of the vapor pressure to the ice saturation vapor pressure, $L_S = 2.838 \times 10^6$ J kg^{-1} is the latent heat of sublimation for ice, $R_v = 461.5$ J kg^{-1} K^{-1} is the specific gas constant for water vapor, $k_a = 0.0224$ J m^{-1} s^{-1} K^{-1} (at $-20\,°\text{C}$) is the thermal conductivity of air, and $\mathrm{D}_v = 1.909 \times 10^{-5}$ m^2 s^{-1} (at $-20\,°\text{C}$) is the diffusivity of water vapor in air. Initially the ice crystals grow very rapidly and after 3 seconds they are already in excess of 1 micron in radius. For the remainder of the simulation, for $t > 3$ s, the data is binned logarithmically between 1 micron and 100 microns with $n_r = 500$ in order to obtain a finer binning for the ice crystal growth. The ice crystal distribution $\Gamma(s)$ is normalized after each step. For $t > 3$s, $s = \log_{10}(r)$ where r is now in microns. Crystals with radii exceeding 100 microns are assumed to fall out immediately and are removed from the simulation, although in practice the crystals have already settled to the ground before reaching this size. In the region occupied by droplets, the droplets evaporate to maintain the water vapor pressure at the liquid saturation vapor pressure as the ice crystals consume the water vapor. After the droplets have evaporated the rate of ice crystal growth will drop as the water vapor drops to the ice saturation vapor pressure.

The diffusion of water vapor is modeled with the diffusion equation:

$$\frac{\partial E}{\partial t} = D(z)\left(\frac{\partial^2 E}{\partial x^2} + \frac{\partial^2 E}{\partial z^2}\right) \tag{9}$$

The diffusion equation is solved explicitly by marching in time from an intial condition $E(x,z,t=0)$ with time steps $dt = 1$ s. For an interior element at $\left(x_i = idx,\ z_j = jdz\right)$ the discretized diffusion equation, with $dx = dz$, is given by:

$$E_{i,j}\left(t+dt\right) = E_{i,j}\left(t\right) + 2\left(\frac{\mathrm{D}(z)dt}{dx^2}\right)\left(E_{i+1,j}(t) + E_{i-1,j}(t) + E_{i,j+1}(t) + E_{i,j-1}(t) - 4E_{i,j}(t)\right) \tag{10}$$

The diffusion and subsidence of ice crystals are modeled simultaneously by the diffusion equation with an advection term[28] $v\partial C/\partial x$:

$$\frac{\partial C}{\partial t} = D(z)\left(\frac{\partial^2 C}{\partial x^2} + \frac{\partial^2 C}{\partial z^2}\right) - v\frac{\partial C}{\partial x} \tag{11}$$

where the settling velocity v is a function of the ice crystal radius and given by Stokes Law[27]:

$$v(r) = (\rho_c - \rho_a)\frac{2r^2 g}{9\mu} \tag{12}$$

where ρ_c is the ice crystal density, ρ_a is the air density, and μ is the dynamic viscosity. When calculating the advection term, different elements from the normalized radial distribution Γ settle at different velocities. The advection term is discretized by summing the product of the velocity and Γ over the bins $s_k = \log_{10}(r_k)$. For example, for an internal point at position $\left(x_i = idx,\ z_j = jdz\right)$, with $dx = dz$:

$$\begin{aligned} C_{i,j}\left(t+dt\right) = {} & C_{i,j}\left(t\right) + 2\left(\frac{\mathrm{D}(z)dt}{dx^2}\right)\left(C_{i+1,j}(t) + C_{i-1,j}(t) + C_{i,j+1}(t) + C_{i,j-1}(t) - 4C_{i,j}(t)\right) \\ & - \frac{\sum_{k=0}^{n_r-1} v(r_k)\Gamma_{i,j}(s_k,t)}{2dx}\left[C_{i+1,j}(t) - C_{i-1,j}(t)\right] \end{aligned} \tag{13}$$

In addition to the water vapor and ice crystal concentrations, the normalized ice crystal radius distribution $\Gamma_{i,j}(s)$ is updated at each time step by weighting with the concentrations as they

appear in the discretized diffusion equation. For example, if we denote $\tilde{\Gamma}_{i,j}(s,t+dt)$ as the ice crystal distribution before normalization for an internal point, then Eq. (13) yields:

$$\begin{aligned}\tilde{\Gamma}_{i,j}\left(s_k,t+dt\right) &= C_{i,j}\left(t\right)\Gamma_{i,j}\left(s_k,t\right) \\ &+2\left(\frac{\mathrm{D}(z)dt}{dx^2}\right)\Big[C_{i+1,j}(t)\Gamma_{i+1,j}\left(s_k,t\right)+C_{i-1,j}(t)\Gamma_{i-1,j}\left(s_k,t\right) \\ &+C_{i,j+1}(t)\Gamma_{i,j+1}\left(s_k,t\right)+C_{i,j-1}(t)\Gamma_{i,j-1}\left(s_k,t\right)-4C_{i,j}(t)\Gamma_{i,j}\left(s_k,t\right)\Big] \\ &-\frac{\sum_{k=0}^{n_r-1}v(r_k)\Gamma_{i,j}(s_k,t)}{2dx}\Big[C_{i+1,j}(t)\Gamma_{i+1,j}\left(s_k,t\right)-C_{i-1,j}(t)\Gamma_{i-1,j}\left(s_k,t\right)\Big] \end{aligned} \quad (14)$$

Methods references

24. B. Kochtubajda, E. P. Lozowski (1985). The sublimation of dry ice pellets used for cloud seeding. *J. Clim. Appl. Meteorol.*, 24, 597-605.
25. W. J. Eadie, T. R. Mee (1963). The effect of dry-ice pellet velocity on the generation of ice crystals. *J. Appl. Meteorol.*, 2, 260-5.
26. N. Fukuta (1969). Experimental studies on the growth of small ice crystals. *J. Atmos. Sci.*, 26, 522-31.
27. R. R. Rogers, M. K. Yau (1989). *A Short Course in Cloud Physics*. Butterworth-Heinemann.
28. R. B. Bird, W. E. Stewart, E. N. Lightfoot (1960). *Transport Phenomena*. John Wiley and Sons, Inc.

Acknowledgements

The author gratefully acknowledges Carlos F. M. Coimbra, Sarah Doherty, Hugh Morrison, Philip J. Rasch, and Lynn Russell for helpful discussions.

Competing interests

The author declares no competing interests.

Data availability

The simulation code and the data sets generated and analyzed during the current study are available in the Google Drive repository, https://drive.google.com/drive/u/0/folders/1YrDzhmLcublpX4SYyDNy5W94Jf09XxAL .

Supplementary Files

This is a list of supplementary files associated with this preprint. Click to download.

- Linktosimulationcode.docx